Supplementary Material to

"Typical and anomalous pathways of surface-floating material in the northern North Atlantic and Arctic Ocean"

Agnieszka Herman, Jan Marcin Wesławski

Corresponding author:
Agnieszka Herman
Institute of Oceanology, Polish Academy of Sciences, Sopot, Poland
Email: agaherman@iopan.pl

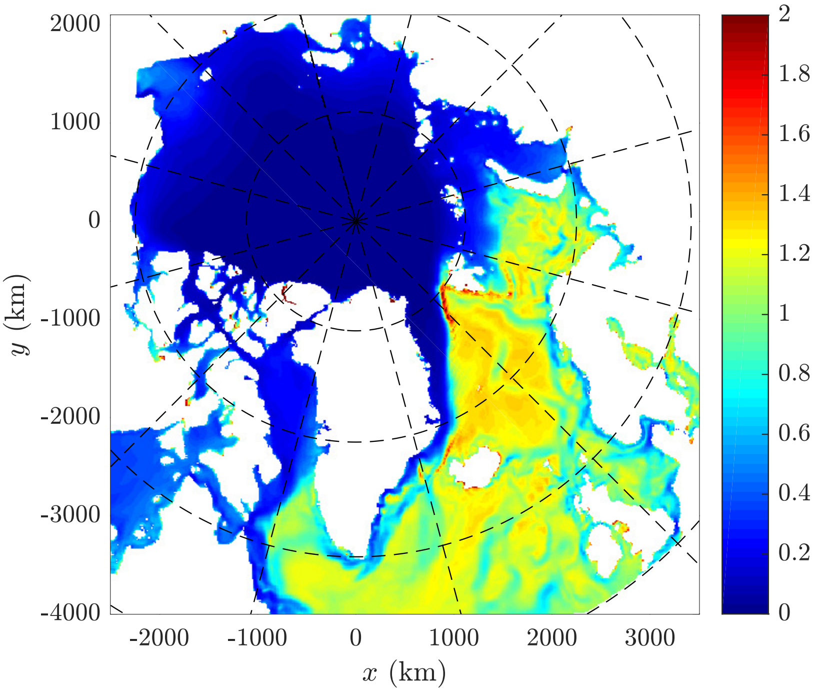

Supplementary Figure 1: The 1993–2020 mean ratio of the Stokes drift amplitude $|\mathbf{u}_S|$ to the amplitude of wind current $|\mathbf{u}_c|$ (see Fig.2c,f,i in the main text).

Supplementary Note S1. The role of the diffusion coefficient K_h

As noted in the main text (see Methods), sensitivity simulations have been performed for trajectories originating at ICE in order to assess the influence of the value of the diffusion coefficient K_h on the modelled particle trajectories. Three values of K_h have been tested, $K_h = 29\ \mathrm{m^2 \cdot s^{-1}}$ (used in the simulations described in the main text), $K_h = 290\ \mathrm{m^2 \cdot s^{-1}}$ and $K_h = 2.9\ \mathrm{m^2 \cdot s^{-1}}$.

Supplementary Fig. 2 shows the corresponding probabilities of drifters reaching from ICE to the remaining 15 destination regions (see also connection matrix in Fig. 3a in the main text). As can be seen, for all connections with probabilities higher than 0.1%, their values obtained with the three different K_hs are very similar and remain at the level below 1%. Only connections to FJL, GLN and SBW show larger differences, but those destinations are reached by too few drifters for the statistics to be robust (this is the reason those connections are not analyzed in the discussion in the main text). Analogously, the statistics of the minimum and median drift times for connections from ICE remain largely unaffected Supplementary Fig. 3), with the same exceptions as those described above – although, as expected, overall larger K_h lead to slightly shorter times, and the differences in times obtained with different K_h get more pronounced for longer trajectories, e.g., those to BEI or SVA.

The time series of release and landing events, shown for two examples (NOR and SVA) in Supplementary Fig. 4, exhibit some differences for different K_h – again, as expected, the peaks in those time series are generally smaller for smaller K_h and *vice versa* – but, crucially, the differences are very small between $K_h = 29\ \mathrm{m^2 \cdot s^{-1}}$ and $K_h = 290\ \mathrm{m^2 \cdot s^{-1}}$, the two values that can be seen as limits of K_h reported in the literature.

Overall, the results of the sensitivity tests show rather limited influence of K_h on the statistical properties of the modelled trajectories, suggesting that the results obtained with $K_h = 29\ \mathrm{m^2 \cdot s^{-1}}$, discussed in the main body of this paper, can be treated as representative for a wide range of realistic values of the diffusion coefficient.

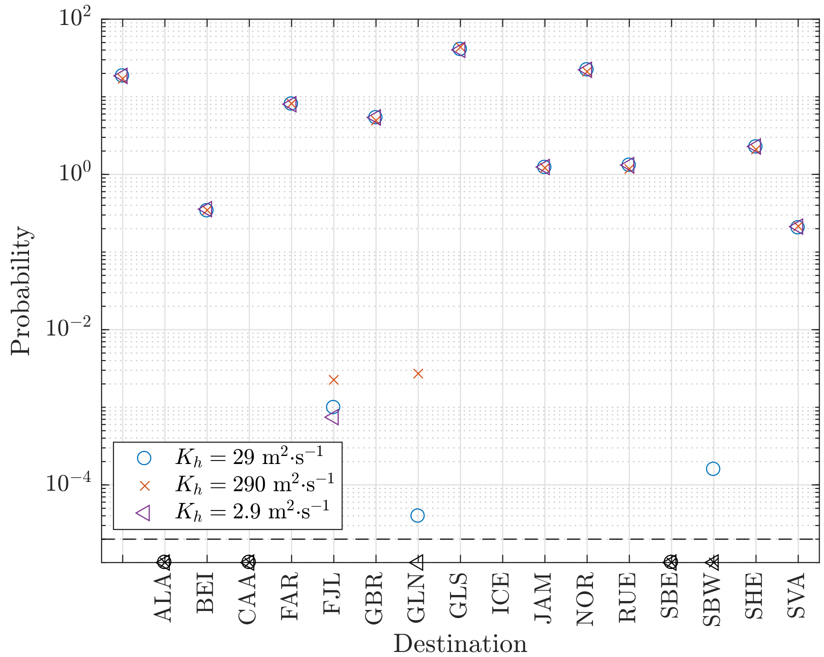

Supplementary Figure 2: The influence of K_h on the fraction (in percent) of particles from ICE reaching the 15 destination regions considered. The left-most, unlabelled value corresponds to particles that left the domain of study or are still adrift after the maximum time of 3 years.

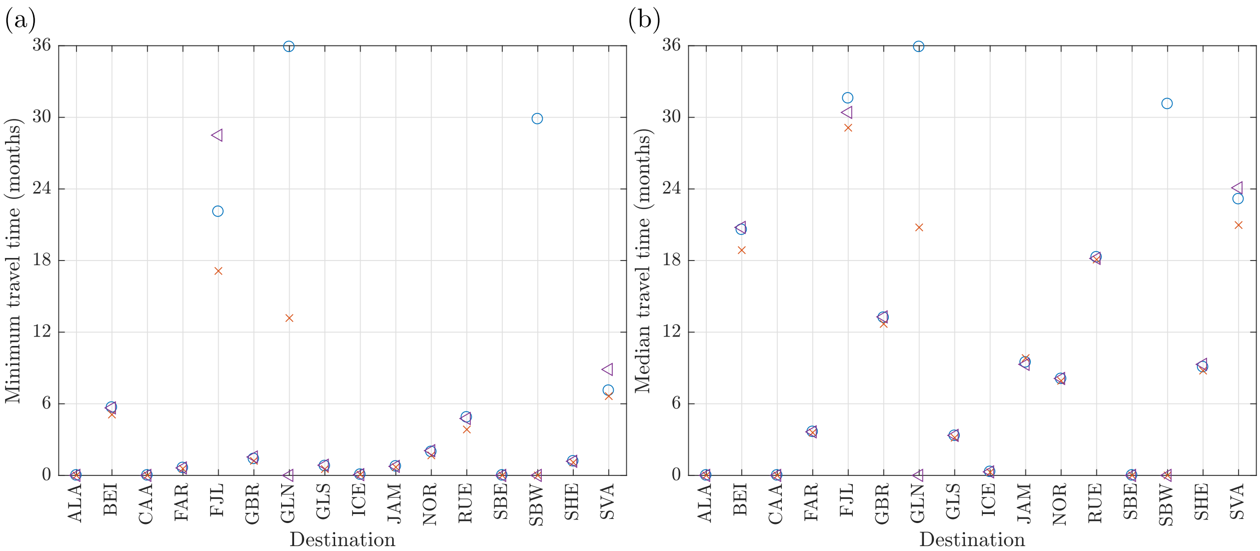

Supplementary Figure 3: The minimum (a) and median (b) drift time in months between ICE and the other 15 regions considered. Meaning of symbols as in Supplementary Fig. 2.

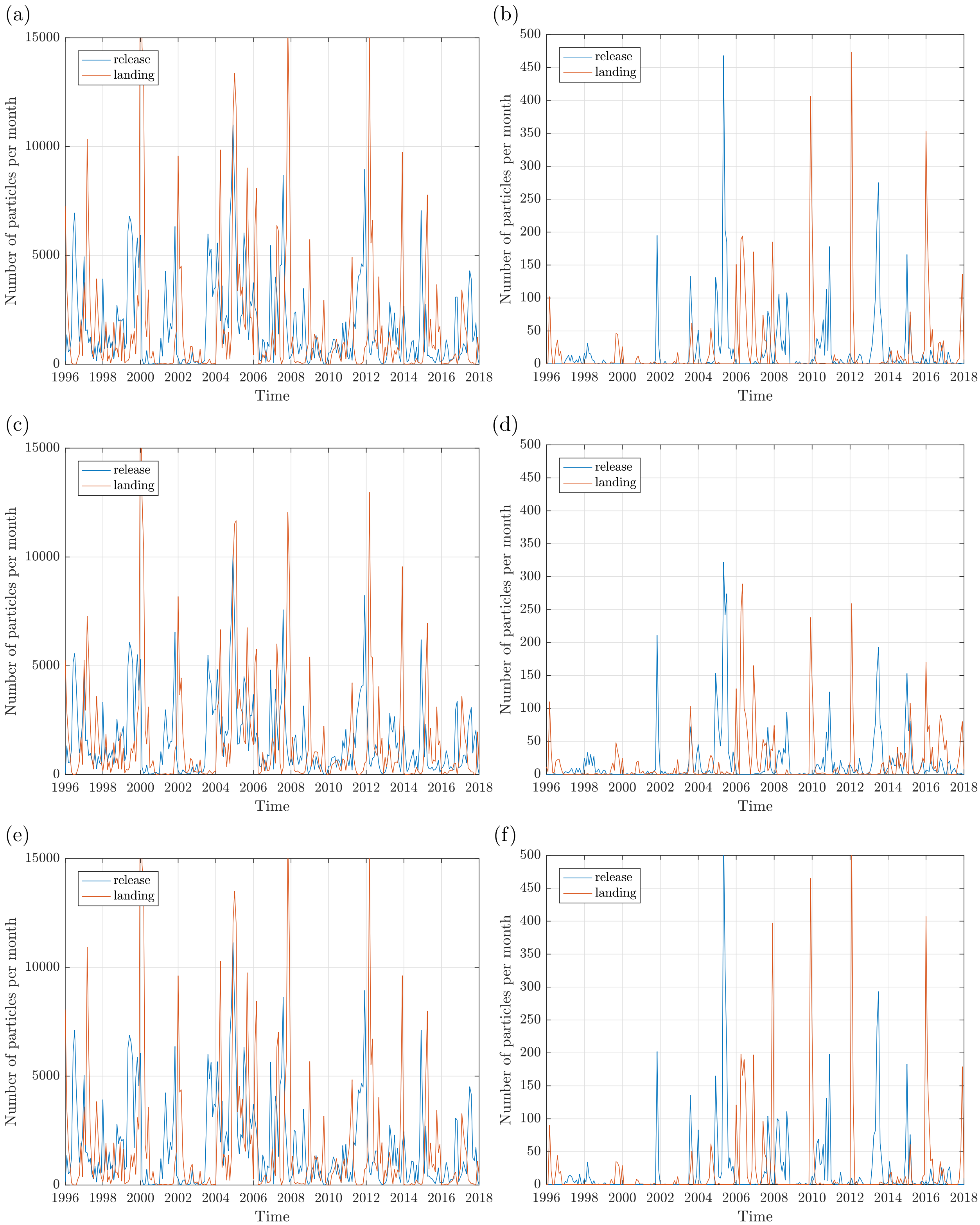

Supplementary Figure 4: Time series of monthly release (blue) and landing (red) events for particles originating at ICE and reaching NOR (a,c,e) and SVA (b,d,f). Results obtained with $K_h = 29$ $m^2 \cdot s^{-1}$ (a,b), $K_h = 290$ $m^2 \cdot s^{-1}$ (c,d) and $K_h = 2.9$ $m^2 \cdot s^{-1}$ (e,f). Note different ranges of the y-axis in (a,c,e) and (b,d,f).

Supplementary Note S2. Atmospheric circulation indices

Supplementary Figs. 5 and 6 show the spatial patterns and the corresponding time series, respectively, of the four large-scale atmospheric circulation indices used in the main text to construct predictors of GBR→FAR and GBR→ICE transport events.

Supplementary Figs. 7 and 8 show connection matrices, analogous to those in Fig. 3 in the main paper, with colours coding corresponding to linear correlation coefficients between the time series of the four atmospheric circulation indices (a–d) and the monthly number of particles released and landed, respectively.

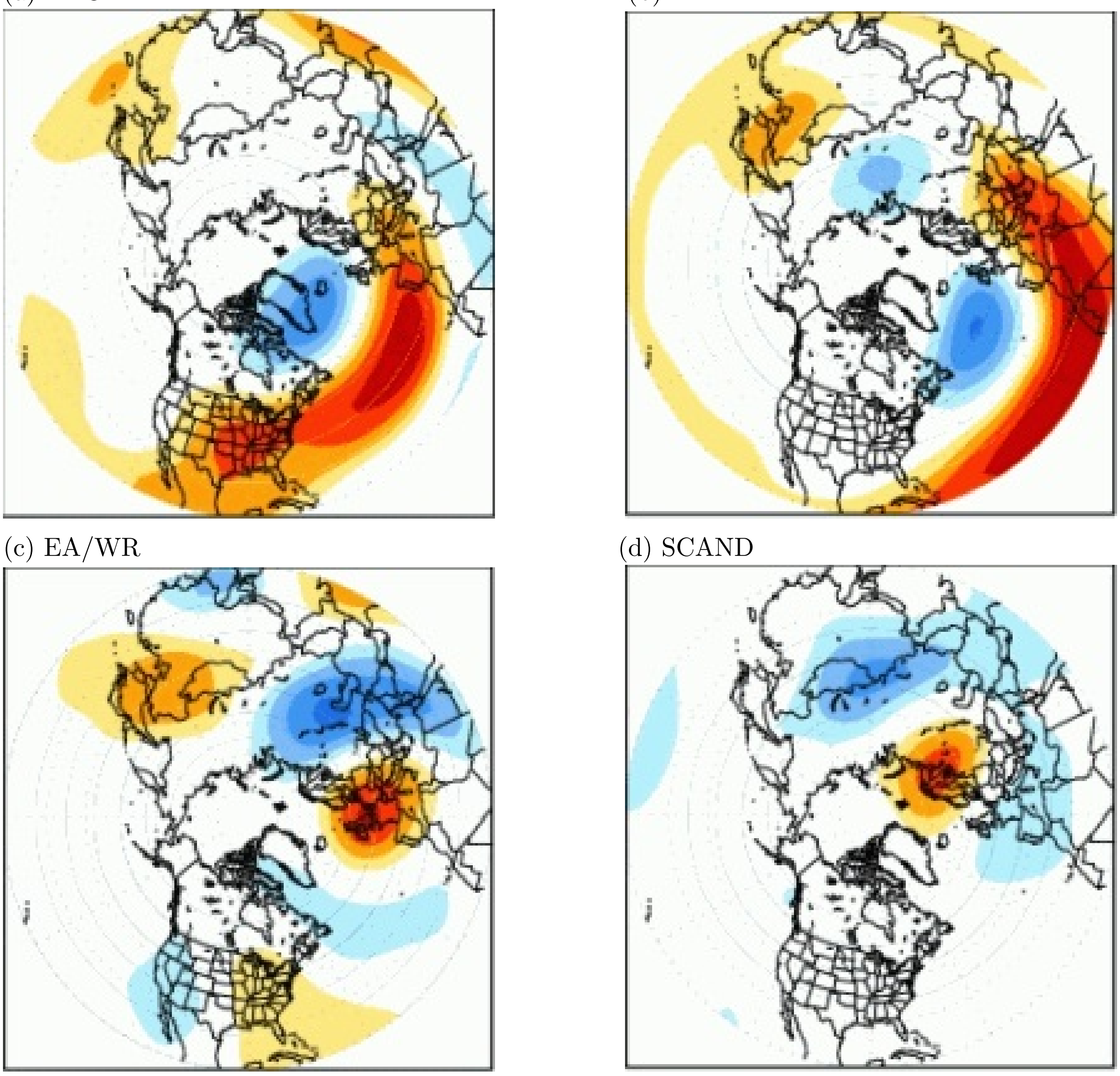

(a) NAO (b) EA (c) EA/WR (d) SCAND

Supplementary Figure 5: Spatial patterns (for the month of January) associated with the four atmospheric circulation indices active over the North Atlantic and the European Arctic. Positive/negative values are shown in red/blue. Source: NOAA Climate Prediction Center, `https://www.cpc.ncep.noaa.gov/data/teledoc/telecontents.shtml`.

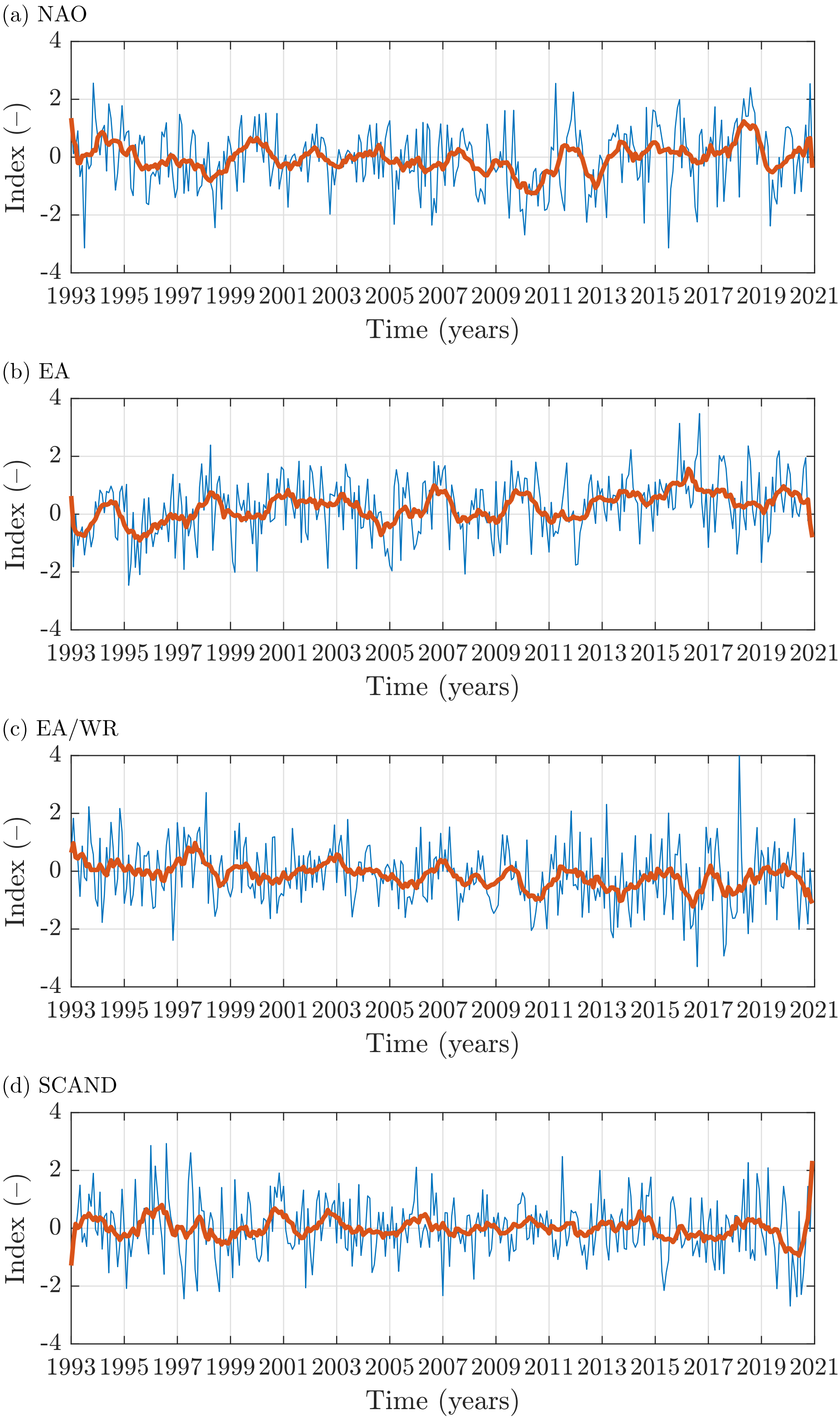

Supplementary Figure 6: Time series of monthly mean (blue) and 12-month smoothed (red) atmospheric circulation indices: NAO (a), EA (b), EA/WR (c) and SCAND (d). Data source: NOAA Climate Prediction Center, `https://www.cpc.ncep.noaa.gov/data/teledoc/telecontents.shtml`.

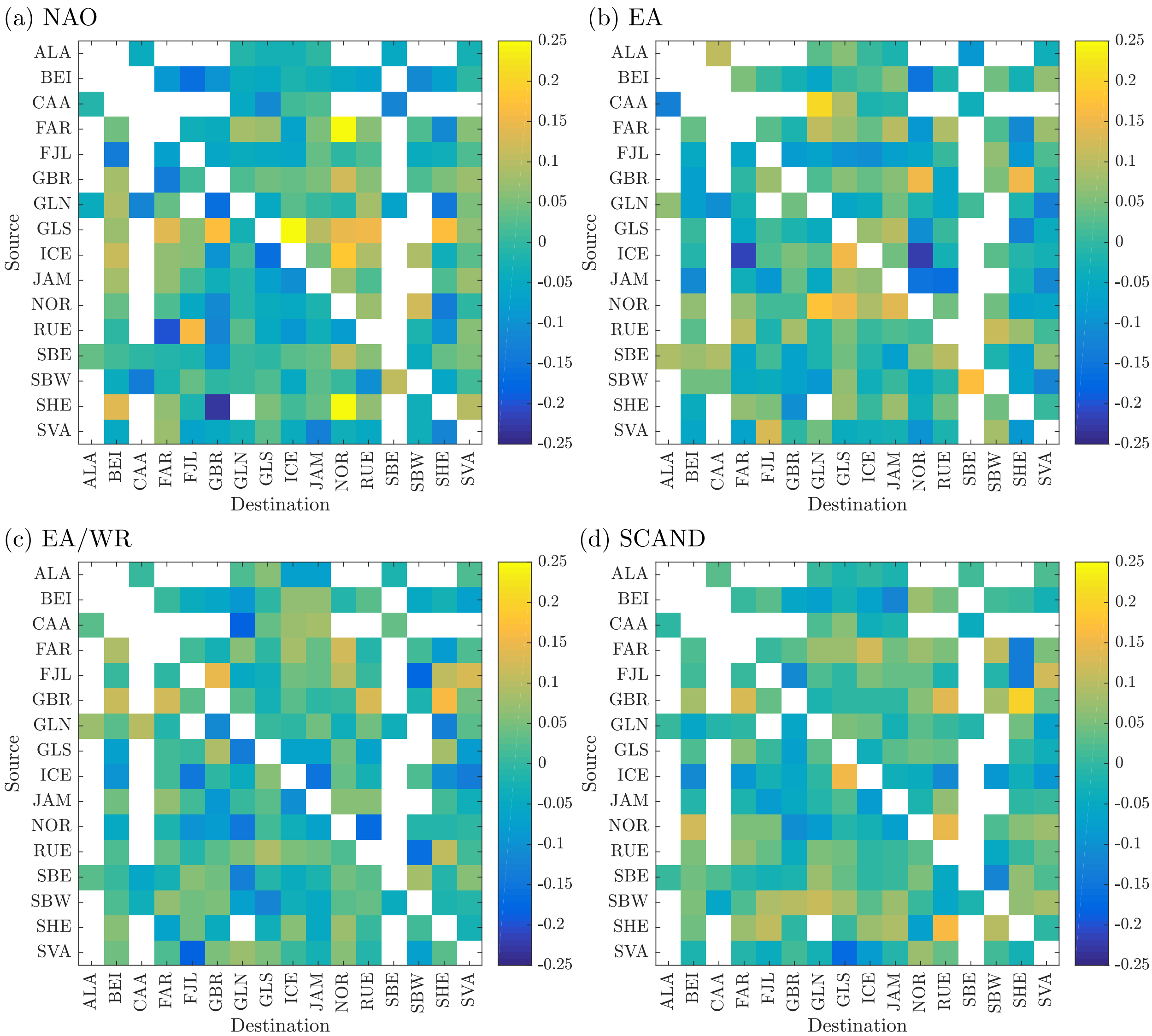

Supplementary Figure 7: Correlation coefficients (for all source–destination pairs) between monthly number of particles released from a given source and the four atmospheric circulation indices analyzed.

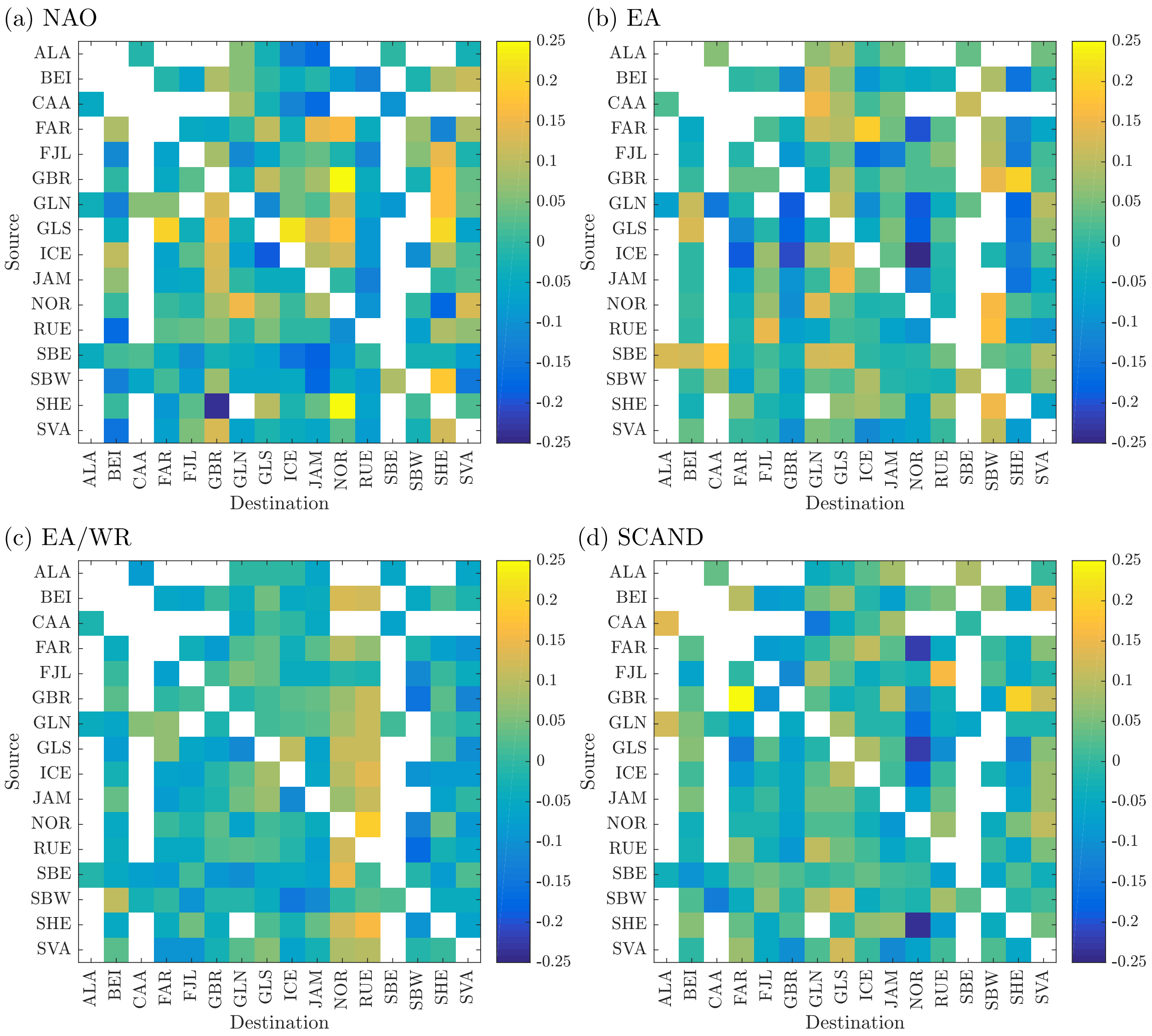

Supplementary Figure 8: As in Fig. 7, but for monthly landing times.

Supplementary Note S3. Spatial distribution of drift material

Supplementary Figs. 9–11 show maps of final positions of all particles released from the 16 regions considered (see main text for a discussion).

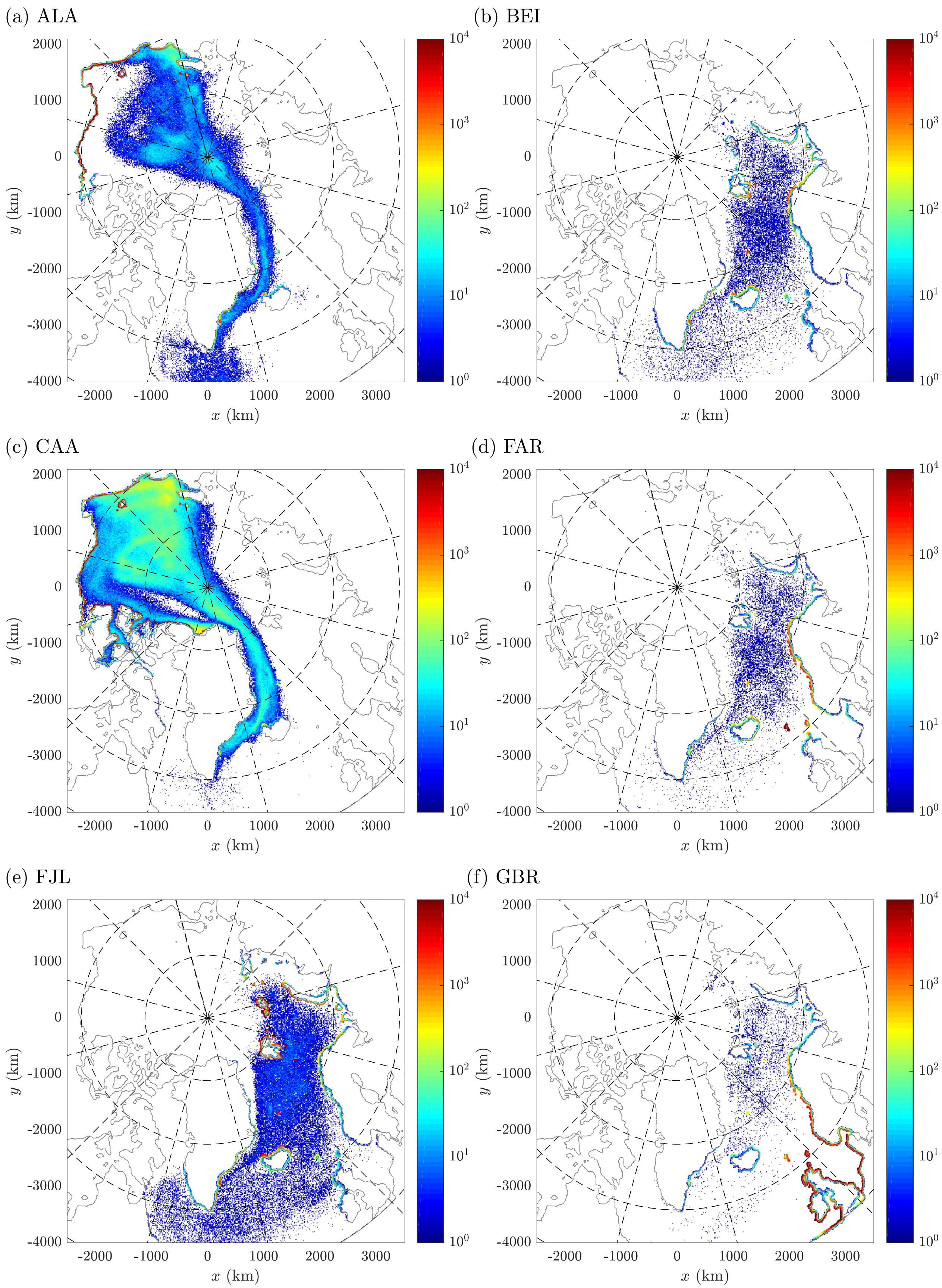

Supplementary Figure 9: Maps of the spatial density of final positions of all particles released from ALA, BEI, CAA, FAR, FJL, GBR (a–f) in the period 1993–2017 (in number of particles per grid cell, i.e., $\sim$156 km^2). The color scale is logarithmic, grid cells with no particles are white.

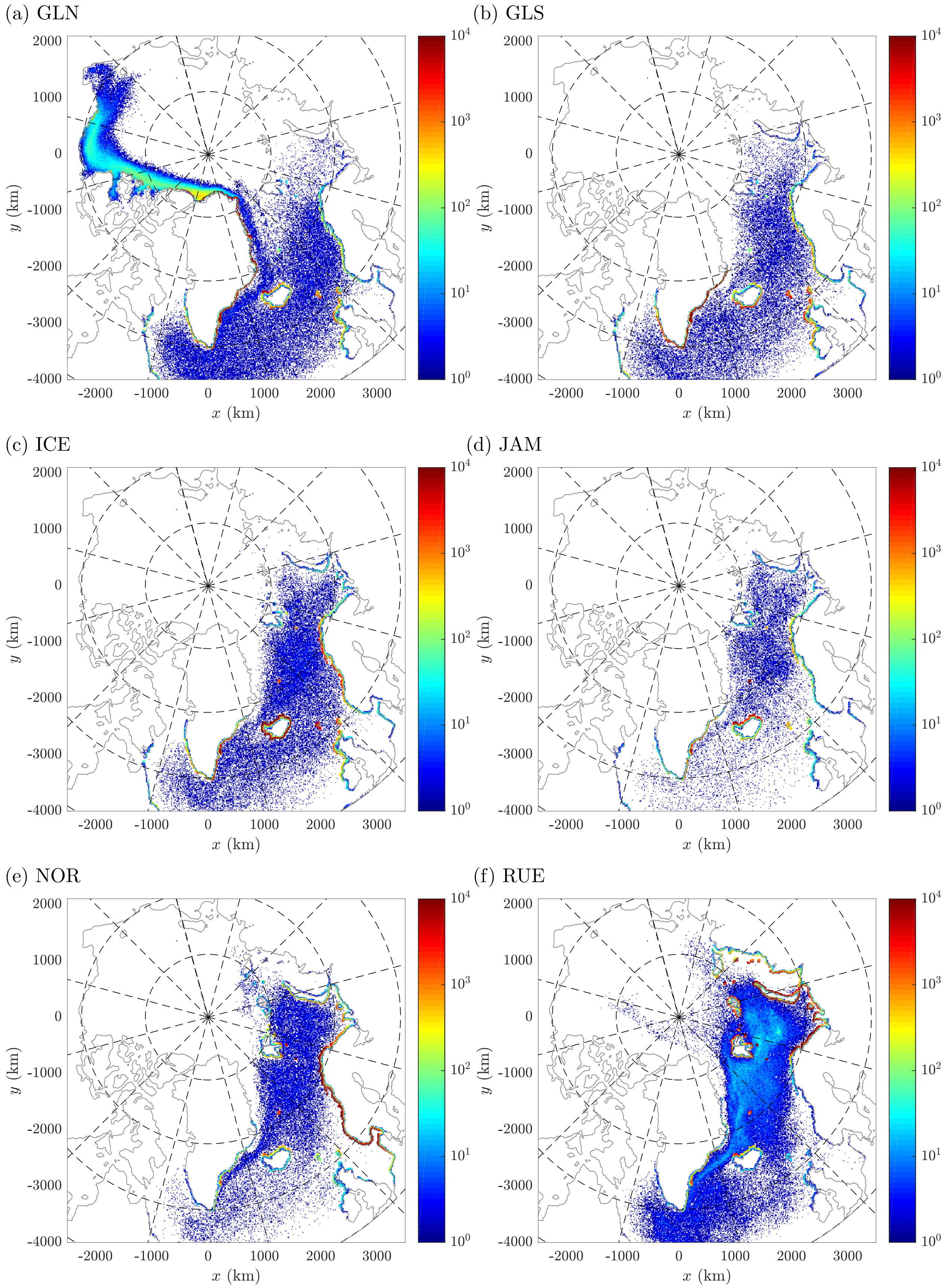

Supplementary Figure 10: As in Supplementary Fig. 9, but for particles released from GLN, GLS, ICE, JAM, NOR and RUE (a–f).

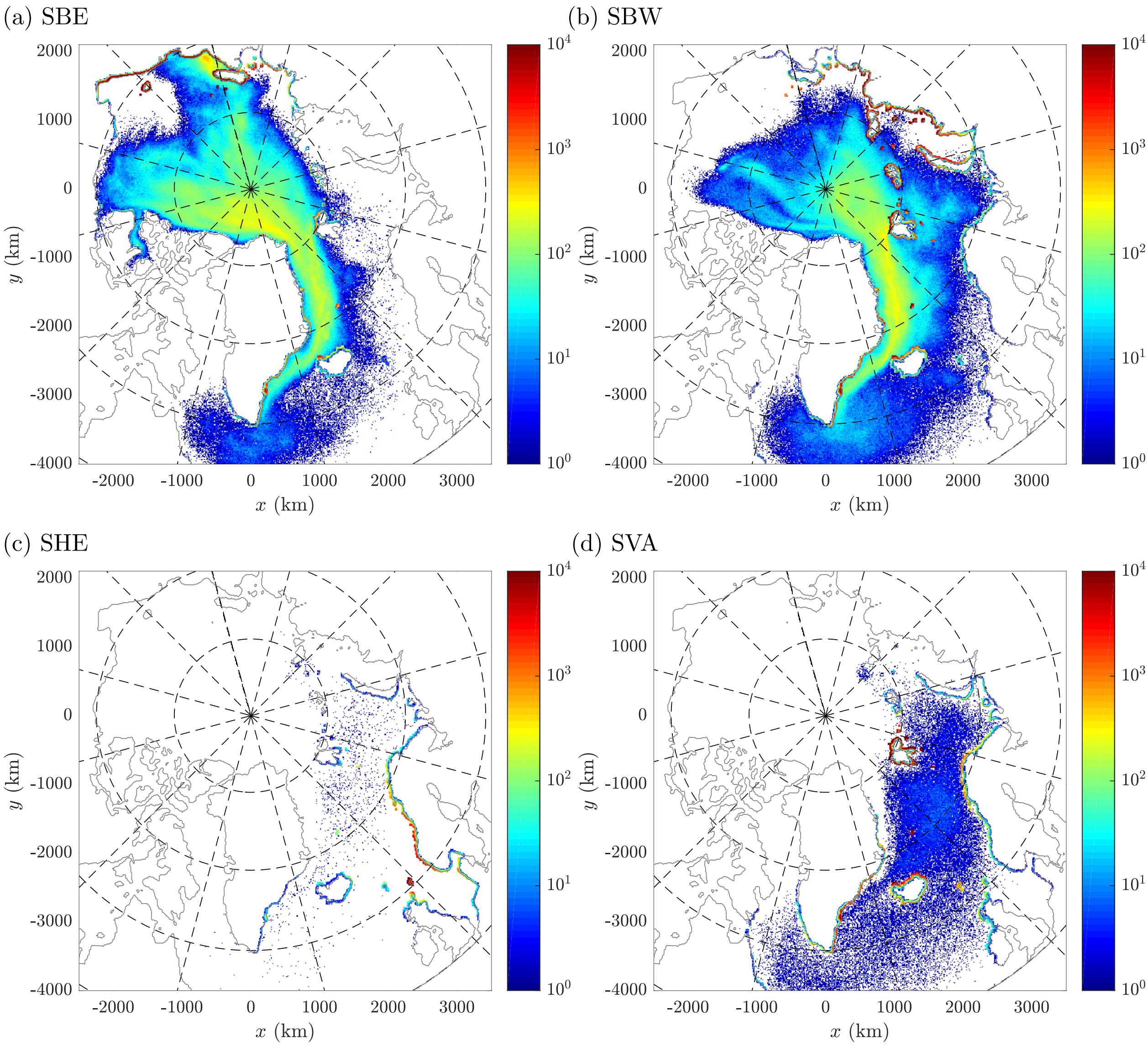

Supplementary Figure 11: As in Supplementary Fig. 9, but for particles released from SBE, SBW, SHE and SVA (a–d).